# Lateral Packing of Mineral Crystals in Bone Collagen Fibrils

Christian Burger,* Hong-wen Zhou,* Hao Wang,† Igors Sics,* Benjamin S. Hsiao,* Benjamin Chu,* Lila Graham,† and Melvin J. Glimcher†

*Department of Chemistry, Stony Brook University, Stony Brook, New York; and †Department of Orthopedic Surgery, Children's Hospital, Harvard Medical School, Boston, Massachusetts

ABSTRACT Combined small-angle x-ray scattering and transmission electron microscopy studies of intramuscular fish bone (shad and herring) indicate that the lateral packing of nanoscale calcium-phosphate crystals in collagen fibrils can be represented by irregular stacks of platelet-shaped crystals, intercalated with organic layers of collagen molecules. The scattering intensity distribution in this system can be described by a modified Zernike-Prins model, taking preferred orientation effects into account. Using the model, the diffuse fan-shaped small-angle x-ray scattering intensity profile, dominating the equatorial region of the scattering pattern, could be quantitatively analyzed as a function of the degree of mineralization. The mineral platelets were found to be very thin (1.5 nm ~ 2.0 nm), having a narrow thickness distribution. The thickness of the organic layers between adjacent mineral platelets within a stack is more broadly distributed with the average value varying from 6 nm to 10 nm, depending on the extent of mineralization. The two-dimensional analytical scheme also leads to quantitative information about the preferred orientation of mineral stacks and the average height of crystals along the crystallographic *c* axis.

## INTRODUCTION

The mineral phase in bone has two major functions (1–3). On one hand, it serves as an ion reservoir, which can rapidly maintain appropriate concentrations of calcium, sodium, magnesium, phosphate, and other ions in the extracellular fluid that are critical for many physiological functions and biochemical reactions. On the other hand, in combination with the organic matrix components (predominantly type I collagen fibrils), within which the mineral phase is embedded, an elegantly arranged three-dimensional ultrastructural composite material is formed that is both lightweight and extremely tough. Both physiological and mechanical functions of bone are affected by the exact size, shape, chemical composition, and crystal lattice structure of the mineral crystals (3,4), by their specific spatial distribution and orientation within the collagen fibrils, and by the degree of mineralization. For instance, the function of the bone composite serving as an ion reservoir requires that the mineral phase must be resorbable very quickly in the body, which is best achieved if the mineral assumes the shape of nanoscale crystals with large surface/volume ratios. Furthermore, the particular spatial arrangement of the composite material at all levels of the anatomical hierarchy of bone substance, i.e., the gross, microscopic, ultrastructural, and molecular levels, provides the specific mechanical properties required to resist many different forces and stresses applied to specific regions of a particular bone as an organ, tissue, and substance without structural failure (3).

After decades of intensive study, it is now clear that the very earliest calcium phosphate solid phase within the collagen fibrils are irregularly shaped, very thin dots (5), typically as small as ~1 nm or less (6). Soon after nucleation, crystal growth occurs and the habit of the mineral crystals changes to very thin, long platelets (6,7). The changes in crystal habit and size are also accompanied by an increase in crystallinity. Needle-shaped crystals were also proposed to be present in bone substance but have since been confirmed to actually be the edge-view of the platelets (for a review, see (3)).

Note that the properties of the mineral crystals also vary as a function of the local rate of bone formation and resorption (bone substance turnover), which in turn determines the age of the crystals locally, that is, the period of time the crystals remain in the bone substance after their initial deposition (4,8). Regions of rapid bone turnover can be located immediately adjacent to regions of very slow bone turnover, with the result that the crystals of adjacent sites at specific microscopic regions of the bone substance may vary greatly in size, shape, local crystal structure, and physico-chemical properties.

The arrangement of mineral crystals along the axis of a collagen fibril, within which they are deposited, mirrors the periodic repeat (~67 nm) present in uncalcified collagen fibrils. These periodic repeats can be visualized by the banding pattern observed in transmission electron microscopy (TEM). Also small-angle x-ray scattering (SAXS) measurement has shown that the equidistant meridional reflections with a long period of ~67 nm are preserved for the mineralized collagen fibrils of bone for various lengths of time after mineralization is initiated (9–11). However, as the concentration of mineral crystals within the collagen fibril increases

*Submitted December 26, 2007, and accepted for publication February 25, 2008.*

Christian Burger and Hong-wen Zhou contributed equally to this work.

Address reprint requests to Benjamin S. Hsiao, E-mail: bhsiao@notes.cc.sunysb.edu; or to Benjamin Chu, E-mail: bchu@notes.cc.sunysb.edu; or Melvin J. Glimcher, E-mail: melvin.glimcher@childrens.harvard.edu.

Editor: Jill Trewhella.



0006-3495/08/08/1985/08 $2.00

doi: 10.1529/biophysj.107.128355

with time, the 67-nm repeat is gradually obliterated, as observed by TEM (8), as well as by SAXS in form of the decreasing number of meridional reflections. The distortion of the original three-dimensional supramolecular packing of collagen molecules in the fibril is also apparent from TEM of very thick ground sections of fully calcified compact bone where the mineral phase occupies the full axial period (12), where eventually both the free volume within the hole regions and the additional volume within the overlap regions are filled with mineral crystals (13).

Little is known about the packing of mineral crystals in the radial direction of the collagen fibril. In electron microscopic studies, individual crystals in tissue sections are difficult to resolve because they are extremely thin, and the collagen fibrils embedding the crystals are densely packed, especially in the heavily mineralized regions of bone. Although electron microscopic tomography and image reconstruction have been utilized to study the three-dimensional spatial arrangement of mineral crystals within the fibril (14), the resolution of this technique (4–6 nm) is well above what is needed to resolve the thickness of mineral platelets.

For more statistically relevant information of crystal dimensions and spatial orientation in a specific volume of bone, the use of SAXS is more suitable. Several attempts have been made to investigate the lateral packing of the mineral crystals in collagen fibrils based on the analysis of the small-angle near-equatorial diffuse scattering feature (i.e., butterfly-pattern) (9,15–18). However, a proper analysis of the scattering data should take into account a priori real-space information obtained from other techniques, such as TEM and atomic force microscopy. The models developed by those authors (15,16) assume that the mineral crystals have needlelike or irregular shapes and are randomly distributed in the cross section of the fibrils, which is inconsistent with the known platelet nature of the mineral crystals (7,19–21). Furthermore, a random distribution within the fibril cross section of the anisotropic platelet cross sections must not allow platelet overlap and, thus, is only feasible if the degree of mineralization is very low.

In this work, the characteristic butterfly-pattern originating from the lateral arrangement of the apatite crystals was analyzed in terms of disordered lamellar stacks of platelet-shaped crystals, intercalated with organic layers having a thickness of a few collagen molecules (see Fig. 1 *a*). This model is more consistent with TEM observations (14,22–24). The thickness distributions of adjacent mineral and organic layers are assumed to be statistically independent, so that the treatment of a one-dimensional density profile along the layer normals (which are preferentially oriented perpendicular to the main fibril axis) resembles the one-dimensional hard-rod fluid model of Zernike and Prins (25) with certain modifications to be discussed below. Preferred orientation effects leading to the actual butterfly-pattern are taken into account (26–28). The analysis leads to the thickness distributions for

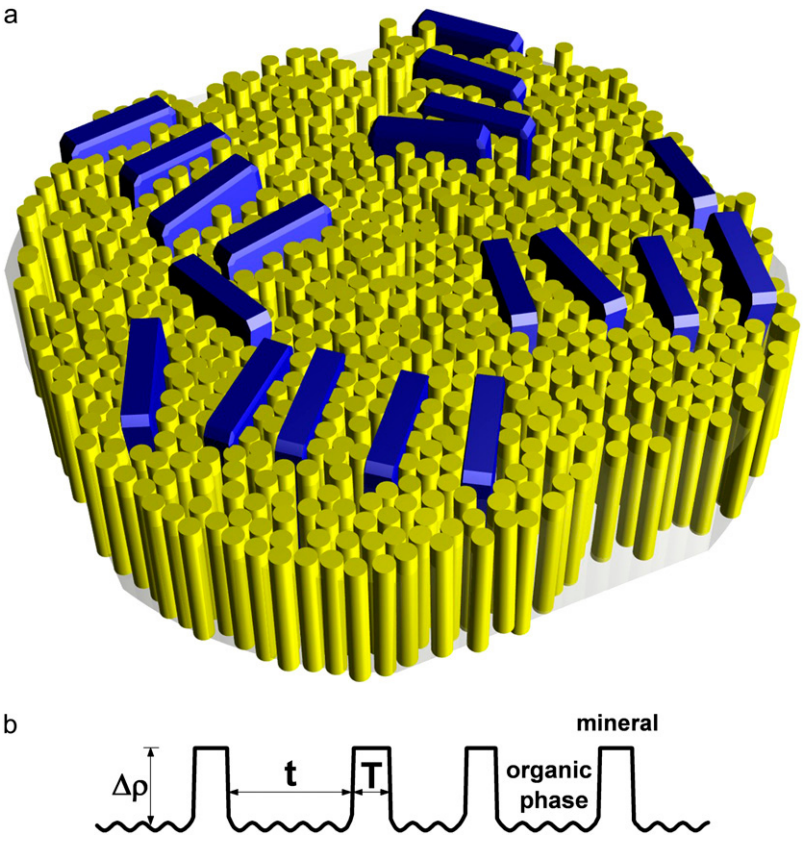


FIGURE 1 (*a*) Schematic illustration of the lateral packing of mineral crystals in the collagen matrix. Thin apatite platelets are aligned nearly parallel within the stacks. The thickness of crystals is typically 2 nm and the width is ~20 nm. The crystal height in the *c*-axis dimension (preferentially aligned about the fibril axis, not visible in this figure) is ~30 nm. (*b*) Electron density projected onto the normal of a stack of mineral platelets. $T$ is the thickness of individual crystals, and $t$ is the thickness of organic layers between the neighboring crystals. The density of the mineral phase can be assumed to be uniform. There are small density fluctuations in the organic phase but their order of magnitude is much smaller than the density contrast ($\Delta\rho$) between the mineral phase and the organic phase.

both the mineral platelets and the intercalated organic layers, the orientation distribution of the mineral stacks, and an estimate for the average height of the mineral crystals, i.e., the dimension parallel to the fibril axis which is known to coincide with the crystallographic *c* axis. The information about the size, shape, preferred orientation, and separation between adjacent crystals is essential for a comprehensive understanding of the three-dimensional spatial relationship between the mineral crystals and their surrounding collagen matrix, on which the mechanical properties and the physiological and biological functions of bone strongly depend.

## PRINCIPLES AND METHODS

The three-dimensional collagen/mineral superstructure has been reviewed elsewhere (28). A schematic representation of the fibril cross section through the hole region is shown in Fig. 1 *a*, illustrating the lateral packing of the mineral crystals in the collagen matrix. In this representation, apatite crystals with a typical height of ~30 nm in the *c*-axis dimension, ~20 nm in width, and 2 nm in thickness (7,19), are arranged into irregular arrays (14,23). Since the average width and height of a crystal are much larger than its thickness, each apatite platelet could be approximated by an infinitely large plate. Under this approximation, the calculation of the scattering intensity from an individual stack of mineral crystals is reduced to a one-dimensional problem, depending only on the one-dimensional density profile projected onto the layer normal direction, as shown in Fig. 1 *b*. The stack can be treated as a two-phase system, one phase being the mineral crystal domain with a large but uniform electron density, and the other being the organic matrix layers embedded between the adjacent crystals. Due to the density difference between collagen molecules and the surrounding fluid within the fibrils, small density fluctuations are expected within the organic matrix layers (but not in the mineral phase), which could give rise to a scattering background more prominent at larger scattering angles. At the present length scales, the organic domains can be considered as homogeneous, confirming the notion of a two-phase system with two homogeneous domains. Furthermore, the density can be assumed to undergo an abrupt change at the mineral/organic phase boundaries so that corrections for a finite density transition profile are not necessary. A theoretical treatment for the scattering from an equivalent system, namely that of the one-dimensional hard-rod fluid, was first given by Zernike and Prins (25). Later, Hermans (29) generalized it for arbitrary thickness distributions and formulated a more elegant expression based on a summable convolution series,

$$I_{1D}(s) = \frac{f}{s^2}\,\mathrm{Re}\left\{\frac{[1-H_1(s)][1-H_2(s)]}{1-H_1(s)H_2(s)}\right\}, \tag{1}$$

where $I_{1D}(s)$ is the intensity in one-dimensional reciprocal space, $s = 2\lambda^{-1}\sin\theta$, is the absolute value of the scattering vector, $\lambda$ is the wavelength, and $2\theta$ is the scattering angle, $s$ is restricted to the direction normal to the layers of the stack, $f$ is a proportionality constant related to the one-dimensional Porod asymptote at large $s$ (i.e., $f = \lim_{s\to\infty} s^2 I_{1D}(s)$), Re{} takes the real part of a complex number, and $H_1(s)$ and $H_2(s)$ are the one-dimensional complex Fourier transforms of the thickness distributions of the two components. Note that Eq. 1 implies an infinite length of the stack in the layer normal direction, i.e., the number of mineral plates in the stack is approximated as infinitely large. A finite number of mineral plates could be introduced, but it would be difficult to separate its effect from the one caused by stacking disorder unless the scattering curve shows higher order maxima, which is not the case for this system.

A TEM study on the lightly mineralized regions of intramuscular herring bone showed that apatite crystals appear to have nearly uniform thickness (23). Therefore, we chose a narrow Gaussian for the thickness distribution of mineral crystals,

$$p_1(T) = \frac{1}{\sqrt{2\pi}\sigma_T}\exp\left(-\frac{(T-\langle T\rangle)^2}{2\sigma_T^2}\right), \tag{2}$$

where $p_1(T)dT$ is the probability of finding a crystal with thickness between $T$ and $T + dT$, $\langle T\rangle$ is the average thickness, and $\sigma_T$ is the standard deviation of the thickness distribution. As a probability density distribution, Eq. 2 is normalized to unity integral. The one-dimensional Fourier transform of $p_1(T)$ is thus

$$H_1(s) = \exp(2\pi i\langle T\rangle s - 2\pi^2\sigma_T^2 s^2). \tag{3}$$

TEM images also show that the separations between adjacent crystals, i.e., the thickness of the intercalated organic layers, have a relatively broader distribution (23). A Γ-distribution was chosen for the thickness distribution of organic layers,

$$p_2(t) = \Gamma(v)^{-1}a^{-v}t^{v-1}\exp(-t/a), \tag{4}$$

where $p_2(t)dt$ is the probability of finding an organic layer with thickness between $t$ and $t + dt$, $\Gamma(v)$ is the Γ-function of argument $v$, $v$ is a dimensionless parameter, and $a$ is a parameter with the dimension of a length. The average thickness of organic layers $\langle t\rangle$ is given by $\langle t\rangle = av$, and the standard deviation of the distribution is $\sigma_t = a\sqrt{v}$. Equation 4 is also normalized. The one-dimensional Fourier transform of $p_2(t)$ is

$$H_2(s) = (1 - 2\pi i a s)^{-v}. \tag{5}$$

Assuming the presence of simple fiber symmetry, the scattering intensity of a perfectly oriented system of stacks, randomly aligned with their layer normals pointing perpendicular to the fiber axis direction, can be written as

$$I(s_{12}, s_3) = \frac{1}{\pi s_{12}} I_{1D}(s_{12}) I_3(s_3), \tag{6}$$

where $s_{12}$ and $s_3$ are components of the reciprocal space vector $\vec{s}$ with $|\vec{s}| = \sqrt{s_{12}^2 + s_3^2}$, $s_{12}$ is perpendicular to the fiber axis, and $s_3$ is in the fiber axis direction. A normalization factor $(2\pi s_{12})^{-1}$ results from the circular average, another factor 2 from $I_{1D}$ touching the averaging circumference at two points, and the longitudinal component $I_3(s_3)$ depends on the averaged size, shape, and possible correlation of the crystals in the fiber axis direction. We found that a Lorentzian function gives the best fit to the measured two-dimensional intensity profile,

$$I_3(s_3) = \frac{1}{w_3}\frac{1}{1 + \pi^2(s_3/w_3)^2}, \tag{7}$$

where $w_3$ is the integral peak width, and its reciprocal value $w_3^{-1}$ is used as an estimate of the average crystal height $H$, assuming that there is no strong correlation from a stack in one hole-zone to the stacks in the neighboring hole-zones along the fibril axis.

Considering the preferred orientation effects, the *c* axes of the apatite crystals are preferentially oriented along the primary bone axis, as indicated by the arc-shaped (002) reflection on the meridian of wide-angle x-ray diffraction (WAXD) patterns (9,10,30,31). Note that the preferred orientation observed by WAXD is a superposition of the preferred orientation of the fibrils with respect to the bone axis and that of the *c* axes of mineral crystals with respect to the axis of the associated fibril (4,30). The latter is usually identified by electron diffraction from individual mineralized collagen fibrils (23,30). The orientation studied by SAXS analysis is similar to that by WAXD, i.e., it refers to the overall orientation of mineral crystals with respect to the bone axis. When taking this preferred orientation into account, scattering from all stacks will no longer be a thin streak on the equator, but spread into a characteristic butterfly-pattern (shown in Fig. 2). The resulting fiber-averaged intensity distribution, $J(s,\phi)$, is given by (26,27)

$$J(s,\varphi) = \int_0^{\frac{\pi}{2}} I(s,\varphi')F(\varphi,\varphi')\sin\varphi' d\varphi', \tag{8}$$

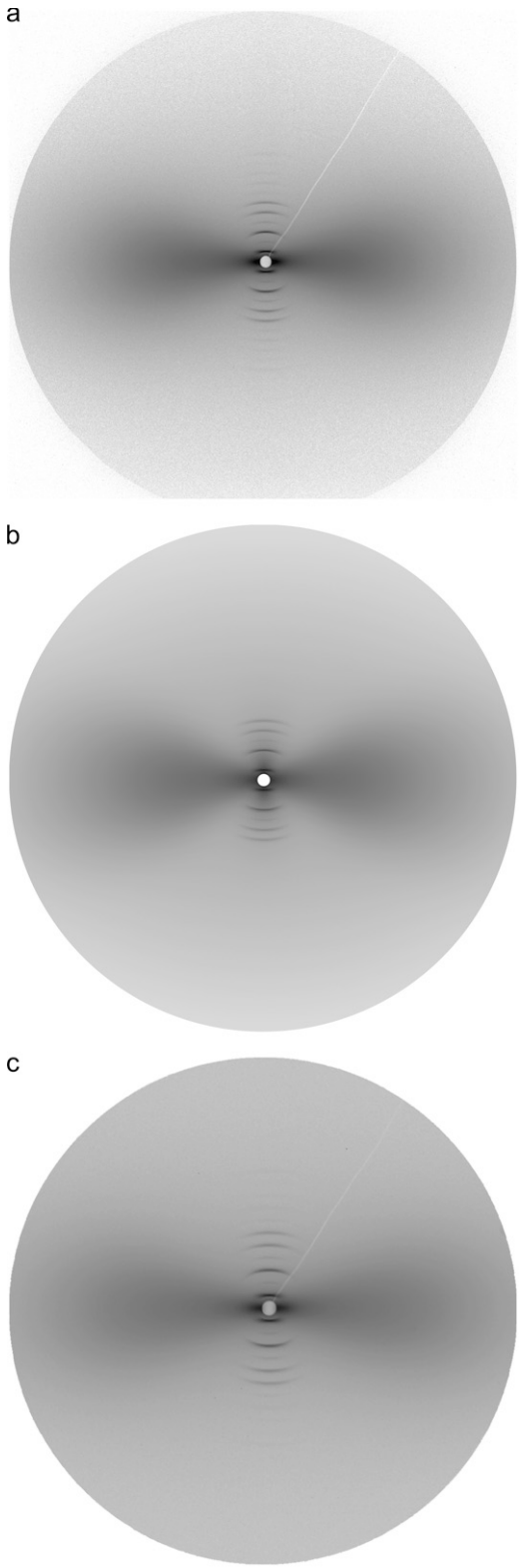


FIGURE 2 (*a*) Measured two-dimensional SAXS pattern from intramuscular shad bone by imaging plate. Sample/detector distance was 1897 mm and the measurement range covered $s = 0.01 \sim 0.38$ nm$^{-1}$. Bone axis is in the vertical direction ($s_3$, meridian). The equator $s_{12}$ is perpendicular to the bone axis. (*b*) Calculated pattern for panel *a*. The total intensity is a combination of the fan-shaped diffuse scattering originating from the lateral packing of mineral crystals in organic matrix (described in this article), and sharp meridional reflections originating from periodic packing of collagen molecules and mineral crystals along the fibril axis (see (28) for details). The corresponding fitting parameters are listed in Data S1, Table 1. (*c*) Diffraction pattern from the same irradiated volume as in panel *a*, but recorded with a CCD camera. Sample/detector distance was 1942 mm and the measurement range covered 0.01 $\sim$ 0.30 nm$^{-1}$.

where $I(s,\phi')$ is the intensity distribution for the perfectly oriented system (Eq. 6) translated into polar coordinates, and $F(\phi,\phi')$ is related to the orientation distribution of the stacks. A detailed analysis and application of Eq. 8 can be found in a separate article (28).

## EXPERIMENTAL

Native intramuscular shad/herring bones were used for all experiments. The bone specimen has roughly a fiber shape with a diameter ~0.5 mm. Information about the sample preparation, x-ray instrumentation, and image processing has been described elsewhere (28,32). In addition to the imaging plates (IP), a charge-coupled device (CCD) x-ray detector (MarUSA, Rayonix, Evanston, IL) was also used to record selected SAXS patterns to confirm the absence of detector-related systematic errors.

The butterfly-pattern was fitted after removing regions that contain meridional reflections. An analytical background was incorporated into the two-dimensional fitting scheme since it cannot unambiguously be separated from the diffuse scattering that is of interest. Various functions (constant, plane, etc.) were tested and it was found that the background shape had a relatively small effect on the final results. The best fitting quality was achieved when an elliptically stretched Pearson type VII function was used ($n$ was fixed at 12 during the fitting),

$$Background = \frac{c_0}{\left(1 + c_1 s_{12}^2 + c_2 s_3^2\right)^n}. \quad (9)$$

TEM cross-sectional images were obtained in a JEM-2011 microscope (JEOL, Tokyo, Japan). Bone samples were fixed in 0.1 M sodium cacodylate-buffered 4% paraformaldehyde and 2% glutaraldehyde solution for 24 h at 4°C, and then subsequently fixed in 1% osmium tetroxide solution for 2 h at 4°C. After being dehydrated through a series of 50%, 70%, 85%, 95%, and 100% ethanol, the samples were infiltrated in 1:1 LR White resin (Ted Pella, Redding, CA) dissolved in ethanol for 24 h and then vacuum-infiltrated with pure LR White. The recovered samples were then embedded in fresh LR White resin (Ted Pella) for 24 h at 50°C. Silver to golden thin sections, prepared by using an ultramicrotome (RMC model MT-X; Boeckeler Instruments, Tucson, AZ), were collected on parlodion-coated grids (Ted Pella), and air-dried. The microtomed sections were typically 70 nm in thickness; therefore, they contained no more than two hole regions in the fibrils' axis direction.

## RESULTS AND DISCUSSION

Fan-shaped diffuse profiles in SAXS patterns from the mineralized portion of intramuscular fish bone were analyzed using the approaches described above. The quality of the fitting was evaluated by comparing an experimental pattern (Fig. 2 *a*) with a calculated pattern (Fig. 2 *b*) from the fitting results. It is shown that the calculated pattern has faithfully reproduced the features of the measured pattern, as indicated more clearly in the three-dimensional relief plots viewed from different perspectives (Supplementary Materials, Data S1, Fig. 1). To ensure the absence of systematic errors introduced by the x-ray detectors, SAXS patterns from the exact same irradiated volume were recorded with two types of detectors (IP and CCD) that have different working mechanisms. Analysis of the patterns acquired with IP (Fig. 2 *a*) and CCD (Fig. 2 *c*) generates two sets of structure parameters that agree well with each other (Data S1, Table 1), proving that detector-related systematic errors are negligible.

### Mineral crystal packing in collagen matrix

Unlike the bones in higher vertebrates, in which regions of newly formed osseous tissue are mixed with regions of the aged tissue on a microscopic scale (i.e., much smaller than the typical size of an x-ray beam), the intramuscular shad/herring bone shows a gradually increased degree of mineralization along the bone axis (23), thus allowing us to use x-ray scattering and diffraction techniques to study the structural evolution of bone at different developing stages. SAXS patterns from spots at different degrees of mineralization were analyzed, and the results are listed in Table 1. The average thickness of the mineral crystals $\langle T \rangle$ shows a monotonic increase from ~1.5 nm at the lightly mineralized regions to ~2.0 nm at the heavily mineralized regions. However, the thickness distribution of the mineral crystals $\sigma_T$ at each developing stage is relatively narrow (see Fig. 3, *left*), indicating that bone apatite crystals of a similar age have a nearly uniform thickness. The average separation between the neighboring crystals $\langle t \rangle$ decreases from ~10 nm at the lightly mineralized regions to ~6 nm at the heavily mineralized regions, suggesting that the packing of mineral crystals in the collagen matrix becomes more dense as the mineralization progresses. However, the separations between adjacent crystals within a mineral stack are broadly distributed (see Fig. 3, *right*). The average crystal height $H$, i.e., the dimension along the *c*-axis direction, also shows an increase from the lightly mineralized region (~30 nm) to the heavily mineralized regions (~50 nm). The overall orientation of the mineral stacks defined by the Hermans' orientation factor (28,33) remains unchanged.

**TABLE 1 Structural parameters of intramuscular shad bone as a function of the degree of mineralization**

| Sample position | $\langle T \rangle$ (nm) | $\sigma_T$ (nm) | $\langle t \rangle$ (nm) | $\sigma_t$ (nm) | $H$ (nm) | Hermans' orientation factor |
|---|---|---|---|---|---|---|
| LM01 | 1.48(2) | 0.08(1) | 10.4(2) | 6.24(3) | 29.9(2) | 0.842(1) |
| LM02 | 1.62(1) | 0.06(1) | 7.79(3) | 4.85(2) | 34.8(2) | 0.850(1) |
| HM03 | 1.92(1) | 0.05(1) | 6.69(1) | 3.80(2) | 50.7(2) | 0.837(1) |
| HM04 | 1.96(1) | 0.06(1) | 6.15(2) | 3.63(2) | 54.3(1) | 0.852(1) |
| HM05 | 2.00(1) | 0.04(1) | 6.89(1) | 3.99(2) | 51.5(1) | 0.835(1) |

*LM*, lightly mineralized; *HM*, heavily mineralized; $\langle T \rangle$ is the average thickness of the mineral crystals; $\sigma_T$ is the standard deviation of the mineral crystal thickness; $\langle t \rangle$ is the average thickness of the intercalated organic layers; $\sigma_t$ is the standard deviation of the organic layer thickness; and $H$ is the average height of the mineral crystals in the crystallographic *c*-axis direction. Hermans' orientation factor is described in detail in Burger et al. (28).

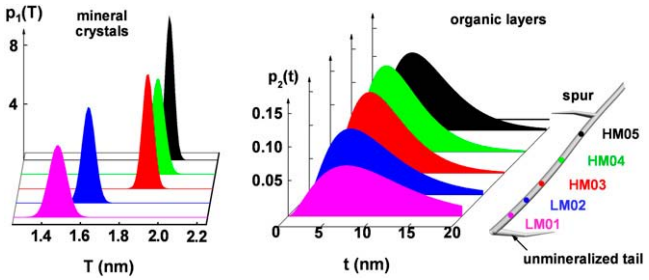


FIGURE 3 Evolution of the mineral crystal packing in the collagen matrix at different degrees of mineralization. The intramuscular shad bone sample (*right*) has roughly a fiber shape with an unmineralized tail at the end and a spur in the middle. The extent of mineralization gradually increases from the interface between the two portions (unmineralized and mineralized) to the spur. The thickness distributions of the mineral crystals are plotted as narrow Gaussians (Eq. 2) and the thickness distributions of the intercalated organic layers are plotted as Γ-distributions (Eq. 4). Note that the scale range for the mineral thickness distribution (*left*) is 1/20 of that for the organic layer thickness distribution (*right*).

Note that the majority of the bone mineral crystals are formed within a confined environment, i.e., the individual collagen fibrils based on which the bone tissues are constructed. The nucleation and crystal growth thus are strongly affected by the three-dimensional supramolecular architecture in the collagen fibrils (30). It has been recently observed that, before mineralization, parallel channels are created within the collagen fibrils by the ordered packing of molecules in the fibril cross section (to be reported elsewhere). The channels are ~1.5 nm in breadth, which is comparable to the thickness of the early mineral crystals. Crystal growth in the thickness dimension is strongly constrained by the breadth of the channels, as indicated by the small increase of the crystal thickness from the lightly mineralized regions to the heavily mineralized regions. On the other hand, the length of the channels extends to more than 50 nm, thus the crystal growth in this dimension (corresponding to the width of the crystal) can reach tens of nanometers.

The parallel arrangement of the channels in unmineralized bone collagen fibrils ensures that the mineral crystals form lamellar stacks rather than being randomly oriented in the cross section of the fibril. For the platelet-shaped crystals, the formation of stacks can achieve higher packing density and therefore improved mechanical strength and stiffness. At the early stages of mineralization, the apatite crystals may be randomly deposited into the parallel channels, thus the sep-

aration between the nearest neighbors, or the thickness of the intercalated organic layers, is expected to have a relatively broad distribution, as depicted in Fig. 3. However, it should be mentioned that the nucleation and growth of a mineral crystal in one channel perturbs the surrounding matrix structure as well as the adjacent channels. Consequently, the packing of mineral platelets does not possess long-range order in the lateral direction. Instead, they form irregular lamellar stacks as schematically shown in Fig. 1.

An early scheme developed by Fratzl and co-workers used a formalism originating from the scattering of microemulsions to describe the scattering behavior of such irregular stacks of mineral platelets (34). It is the nature of such a description that mineral phase and organic phase are treated equivalently, e.g., having the same type of thickness distribution, with only the volume fraction being the essential adjustable parameter. When a 1D section through an isotropic 3D two-phase system is considered and the length distributions of the two types of chords on this 1D section are assumed to be statistically independent from each other and to be given by exponential distributions, then the resulting autocorrelation function of the 3D isotropic two-phase system is an exponential function with a simple closed-form Fourier transform, and the model is known as the Debye-Bueche random two-phase system (35). When the same formalism in terms of statistical independence and two exponential length distributions is applied to the present 1D problem of the stack normal density profile, the resulting 1D autocorrelation function is likewise an exponential with simple closed-form Fourier transform. This 1D version of the Debye-Bueche random two-phase system is considered in Fratzl et al. (34), together with a correlated case also based on exponential distributions. As shown above, we find that the thickness distributions for mineral and organic phase, respectively, are quite different, in a way not sufficiently described by the volume fraction alone, and that an exponential distribution cannot adequately model the thickness distribution of the mineral platelets.

## Comparison with TEM results

TEM cross-section images (Fig. 4) for the lightly mineralized collagen fibrils indicate that apatite crystals have large width/thickness aspect ratios. This observation is consistent with the platelet shape in the three-dimensional space when taking the height of the crystals (~30 nm) into account. The mineral platelets are packed into irregular arrays or stacks within the collagen fibrils. The width of the mineral crystals measured from TEM images shows a range from 10 nm to 50 nm, with an average value ~30 nm. The results also agree well with early measurements for isolated bone apatite crystals (19). However, a quantitative evaluation of the mineral crystal thickness from TEM data is difficult. For instance, the *c* axes of the mineral crystals show a preferred orientation with respect to the axis of the associated fibril and, thus, cannot be aligned to the electron beam simultaneously (3,23,30). When the *c* axis of a crystal is not parallel to the electron beam, the profile of the crystal projected onto the TEM image (showing as a *dark line*) will become thicker, especially in the thickness dimension. Therefore, direct measurement for the crystal thickness from a TEM cross-sectional image will get overestimated values. Fig. 4 shows that the short dimension of the dark lines ranges from 2.1 nm to 3.3 nm, which is larger than the average crystal thickness (~1.5 nm in the lightly mineralized region) determined from the SAXS analysis. Giving an average crystal height of ~30 nm, the tilt of the crystallographic *c* axes to the electron beam is estimated (1–4°). This value is significantly smaller than the one determined by electron microscopic tomography (15–20°, see (14)), making sure that our assumption for the parallel arrangement of mineral platelets in a stack is a good approximation. Instead of measuring the thickness of the organic layers directly, we estimated the center/center distance between adjacent crystals, i.e., the summation of a crystal thickness $T$ and that of an embedded organic layer $t$. The results show a broad distribution (3.5–10.4 nm) but in general are smaller than those determined from SAXS analysis (~11.9 nm in average). A possible explanation is that the TEM sample preparation process may cause the shrinkage of the organic matrix by dehydration (36,37), in the case where the degree of mineralization is low and the collagen fibrils still consist of a large amount of tissue water.

## Limitations of the model

This analytical scheme is suitable for the case of platelet-shaped apatite crystals packed into near-parallel arrays. The width and height of the crystals must be significantly larger than the thickness so that the approximation of infinitely large plates is

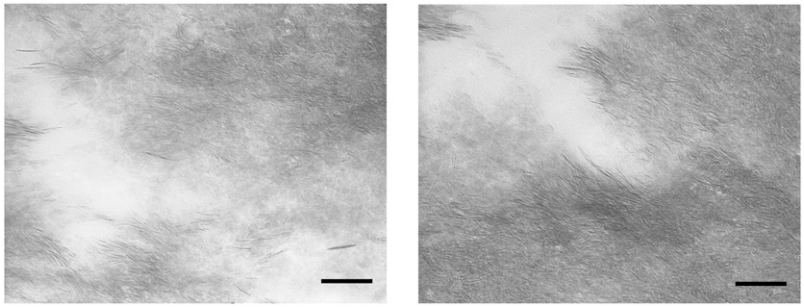

FIGURE 4 TEM images of lightly mineralized intramuscular herring bone. Platelet-shaped mineral crystals are shown as dark lines in the cross section of the fibrils and form near parallel arrays schematically shown in Fig. 1. The scale bar is 100 nm.

well justified. This condition is satisfied for chicken, bovine, mouse, herring, and other species, based on the TEM study of isolated crystals (19) and the tissue sections in this work.

## CONCLUSIONS

In summary, we have developed an effective method to evaluate the lateral packing of mineral crystals in the collagen matrix via quantitative analysis of the butterfly-pattern in small-angle x-ray scattering of intramuscular shad/herring bones. We obtained the thickness distributions for both mineral platelets and intercalated organic layers embedded between them, hence providing more comprehensive information about the spatial arrangement of the mineral phase in the collagen matrix. Such three-dimensional structural information, together with the total volume fraction of the mineral phase, provide much better insights into the structure-property relationships than, e.g., solely the degree of mineralization as presently used in many studies (4). The information obtained in this work can also be used to refine the much simplified one-dimensional structural models developed for calcified collagen fibrils (38), and to find a more precise relationship between the collagen/mineral superstructure and its mechanical properties (39,40). Additionally, we expect it will eventually allow investigations of possible changes in the spatial arrangement of the collagen matrix and embedded mineral phase for bones in pathological conditions.

## SUPPLEMENTARY MATERIAL

To view all of the supplemental files associated with this article, visit www.biophysj.org.

The authors thank Dr. Dufei Fang of Stonybrook Technology and Applied Research for assistance with the x-ray data analysis and Dr. Lixia Rong and Jinglu Chen of Stony Brook University for helping with the synchrotron x-ray measurements. We thank Phillips Brady from the Massachusetts Division of Marine Fisheries for his extended help in procuring live herring and shad fish.

We gratefully acknowledge financial support of this work by the National Institutes of Health (grant No. 5 R01 AG014701-20 to M.J.G., subcontracted to B.S.H. and B.C.), the Peabody Foundation (to M.J.G.), and the Department of Energy (grant No. DEFG0299ER45760 to B.S.H. and B.C) for operation of the X27C beamline at the National Synchrotron Light Source, Brookhaven National Laboratory.

## REFERENCES

1. Glimcher, M. J. 1960. Specificity of the molecular structure of organic matrices in mineralization. *In* Calcification in Biological Systems. R. F. Sogannes, editor. American Association for the Advancement of Science, Washington, DC.
2. Glimcher, M. J. 1984. Recent studies of the mineral phase in bone and its possible linkage to the organic matrix by protein-bound phosphate bonds. *Philos. Trans. R. Soc. Lond. B Biol. Sci.* 304:479–508.
3. Glimcher, M. J. 1998. The nature of the mineral phase in bone: Biological and clinical implications. *In* Metabolic Bone Disease and Clinically Related Disorders. L. V. Avioli, and S. M. Krane, editors. Academic Press, San Diego, CA.
4. Glimcher, M. J. 2006. Bone: nature of the calcium phosphate crystals and cellular, structural, and physical chemical mechanisms in their formation. *Rev. Mineral. Geochem.* 64:223–282.
5. Fitton-Jackson, S. 1957. The fine structure of developing bone in the embryonic fowl. *Proc. Roy. Soc. (London) B.* 14:270–280.
6. Rey, C., H. M. Kim, I. Gerstenfeld, and M. J. Glimcher. 1995. Structural and chemical characteristics and maturation of the calcium-phosphate crystals formed during the calcification of the organic matrix synthesized by chicken osteoblasts in cell-culture. *J. Bone Miner. Res.* 10:1577–1588.
7. Bocciarelli, D. S. 1970. Morphology of crystallites in bone. *Calcif. Tissue Res.* 5:261–269.
8. Glimcher, M. J. 1976. Composition, structure and organization of bone and other mineralized tissue and the mechanism of calcification. *In* Handbook of Physiology: Endocrinology. R. O. Greep and E. B. Astwood, editors. American Association for the Advancement of Science, Washington, DC.
9. Carlstrom, D., and J. B. Finean. 1954. X-ray diffraction studies on the ultrastructure of bone. *Biochim. Biophys. Acta.* 13:183–191.
10. Chen, J.-L., C. Burger, C. V. Krishnan, B. Chu, B. S. Hsiao, and M. J. Glimcher. 2005. In vitro mineralization of collagen in demineralized fish bone. *Macromol. Chem. Phys.* 206:43–51.
11. Zhou, H.-W., C. Burger, S. Igors, B. S. Hsiao, B. Chu, L. Graham, and M. J. Glimcher. 2007. Small-angle x-ray study of the three-dimensional collagen/mineral superstructure in intramuscular fish bone. *J. Appl. Cryst.* 40:s666–s668.
12. Robinson, R. A. 1952. An electron-microscope study of the crystalline inorganic component of bone and its relationship to the organic matrix. *J. Bone Joint Surg.* 34:389–434.
13. Hodge, A. J., and J. A. Petruska. 1963. Recent studies with the electron microscope on ordered aggregates of the tropocollagen molecule. *In* Aspects of Protein Structure. G. N. Ramachandran, editor. Academic Press, New York.
14. Landis, W. J., M. J. Song, A. Leith, L. McEwen, and B. F. McEwen. 1993. Mineral and organic matrix interaction in normally calcifying tendon visualized in three dimensions by high-voltage electron-microscopic tomography and graphic image-reconstruction. *J. Struct. Biol.* 110:39–54.
15. Finean, J. B., and A. Engstrom. 1953. The low-angle scatter of x-rays from bone tissue. *Biochim. Biophys. Acta.* 11:178–189.
16. Fratzl, P., N. Fratzl-Zelman, and K. Klaushofer. 1993. Collagen packing and mineralization. *Biophys. J.* 64:260–266.
17. Fratzl, P. 1994. Statistical model of the habit and arrangement of mineral crystals in the collagen of bone. *J. Stat. Phys.* 77:125–143.
18. Fratzl, P., S. Schreiber, and K. Klaushofer. 1996. Bone mineralization as studied by small-angle x-ray scattering. *Connect. Tissue Res.* 34:247–254.
19. Kim, H.-M., C. Rey, and M. J. Glimcher. 1995. Isolation of calcium-phosphate crystals of bone by nonaqueous methods at low temperature. *J. Bone Miner. Res.* 10:1589–1601.
20. Eppell, S. J., W. Tong, J. L. Katz, L. Kuhn, and M. J. Glimcher. 2001. Shape and size of isolated bone mineralites measured using atomic force microscopy. *J. Orthop. Res.* 19:1027–1034.
21. Tong, W., M. J. Glimcher, J. L. Katz, L. Kuhn, and S. J. Eppell. 2003. Size and shape of mineralites in young bovine bone measured by atomic force microscopy. *Calcif. Tissue Int.* 72:592–598.
22. Traub, W., T. Arad, and S. Weiner. 1989. Three-dimensional ordered distribution of crystals in turkey tendon collagen-fibers. *Proc. Natl. Acad. Sci. USA.* 24:9822–9826.
23. Lee, D. D., and M. J. Glimcher. 1991. Three-dimensional spatial relationship between the collagen fibrils and the inorganic calcium phosphate crystals of pickerel (*Americanus americanus*) and herring (*Clupea harengus*) bone. *J. Mol. Biol.* 217:487–501.
24. Zylberberg, L., W. Traub, V. De Buffrenil, F. Allizard, T. Arad, and S. Weiner. 1998. Rostrum of a toothed whale: ultrastructural study of a very dense bone. *Bone.* 23:241–247.
25. Zernike, F., and J. A. Prins. 1927. X-ray diffraction from liquids. *Zeits. f. Physik.* 41:184–194.

26. Ruland, W., and H. Tompa. 1968. The effect of preferred orientation on the intensity distribution of (hk) interferences. *Acta Crystallogr. A.* 24:93–99.

27. Ruland, W. 1977. Elimination of the effect of orientation distribution in fiber diagrams. *Colloid Polym. Sci.* 255:833–836.

28. Burger, C., H.-W. Zhou, S. Igors, B. S. Hsiao, B. Chu, L. Graham, and M. J. Glimcher. 2008. SAXS study of intramuscular fish bone: collagen fibril superstructure determined from equidistant meridional reflections. *J. Appl. Cryst.* 41:252–261.

29. Hermans, J. J. 1944. Concerning the influence of grid disturbances on the x-ray pattern, particularly in gels. *Rec. Trav. Chim. Pays-Bas.* 63: 211–218.

30. Glimcher, M. J. 1959. Molecular biology of mineralized tissues with particular reference to bone. *Rev. Mod. Phys.* 31:359–393.

31. Engstrom, A. 1972. Aspects of the molecular structure of bone. *In* The Biochemistry and Physiology of Bone. G. H. Bourne, editor. Academic Press, New York.

32. Chu, B., and B. S. Hsiao. 2001. Small-angle x-ray scattering of polymers. *Chem. Rev.* 101:1727–1761.

33. Hermans, J. J., P. H. Hermans, D. Vermaas, and A. Weidinger. 1946. Quantitative evaluation of orientation in cellulose fibers from the x-ray fiber diagram. *Recl. Trav. Chim. Pays-Bas-J. Roy. Neth. Chem. Soc.* 65:427–447.

34. Fratzl, P., H. S. Gupta, O. Paris, A. Valenta, P. Roschger, and K. Klaushofer. 2005. Diffracting ''stacks of cards''—some thoughts about small-angle scattering from bone. *Prog. Colloid Polym. Sci.* 130:33–39.

35. Debye, P., and A. M. Bueche. 1949. Scattering by an inhomogeneous solid. *J. Appl. Phys.* 20:518–525.

36. Eikenberry, E. F., B. Brodsky, and D. A. D. Parry. 1982. Collagen fibril morphology in developing chick metatarsal tendons. 1. X-ray diffraction studies. *Int. J. Biol. Macromol.* 4:322–328.

37. Eikenberry, E. F., B. Brodsky, A. S. Craig, and D. A. D. Parry. 1982. Collagen fibril morphology in developing chick metatarsal tendon. 2. Electron microscopy studies. *Int. J. Biol. Macromol.* 4:393–398.

38. Jäger, I., and P. Fratzl. 2000. Mineralized collagen fibrils: a mechanical model with a staggered arrangement of mineral particles. *Biophys. J.* 79:1737–1746.

39. Gao, H., B. Ji, I. L. Jäger, E. Arzt, and P. Fratzl. 2003. Materials become insensitive to flaws at nanoscale: lessons from nature. *Proc. Natl. Acad. Sci. USA.* 100:5597–5600.

40. Ji, B., and H. Gao. 2004. Mechanical properties of nanostructure of biological materials. *J. Mech. Phys. Solids.* 52:1963–1990.